Conf-9106194 -5

LA-UR -91-2827

LA-UR--91-2827

DE91 017829

Los Alamos National Laboratory is operated by the University of California for the United States Department of Energy under contract W-7405-ENG-36.

MASTER

TITLE: *Single- and Double-Charge Exchange at Low Pion Energies*

AUTHOR(S): Helmut W. Baer

SUBMITTED TO: Proceedings of the International Workshop on Pions in Nuclei, June 3-9, 1991, Peniscola, Spain

SINGLE- AND DOUBLE-CHARGE EXCHANGE AT LOW PION ENERGIES[†]

HELMUT W. BAER
Los Alamos National Laboratory
Los Alamos, NM 87545, USA

ABSTRACT

A review is given of pion single- and double-charge exchange reactions at incident energies of 25 to 65 MeV leading to isobaric analog states, and in the case of double-charge exchange leading to the ground state of the residual nucleus. The crucial role of the higher nuclear transparency at low pion energies for the analysis of the data in terms of single and double scattering is demonstrated. The large effects on double-charge exchange produced by the spatial correlations in nuclear wave functions are evident. The data on $1f_{7/2}$ nuclei at 35 MeV are used to establish the general validity of a shell-model-based two-amplitude model for these transitions. Recent measurements of the energy dependence between 25 and 65 MeV of double-charge exchange cross sections at forward angles are presented and discussed.

1. Introduction

There has been some fairly nice progress in the last few years in understanding the role played by two-nucleon (2-N) correlations in low-energy double-charge exchange scattering (DCX). Underlying this success is the relatively weak π-N coupling at low energies. Evidence for this weak coupling comes from single charge-exchange (SCX) data on transitions to isobaric-analog states (IAS). At low energies the cross sections for these states reflect directly the energy dependence of the free π-N charge exchange cross sections. For DCX reactions, the high pion penetration at low energies produces a large role for 2-N correlations in the double scattering process. Particularly informative have been the transitions leading to double-isobaric analog states (DIAS) and to the ground states (GS) for nuclear targets with $T \geq 2$. Analysis of the considerable body of data on $1f_{7/2}$ shell nuclei at low pion energies shows rather convincingly that the spatial correlations implicit in shell-model wave functions play a major role in shaping DCX cross sections. What is new in the low-energy studies is the clarity with which the two-body correlations are probed.

[†] Invited talk given at the International Workshop on Pions in Nuclei, June 3–8, 1991, Peniscola, Spain.

2. Some Features of π-N Charge Exchange Scattering

It is quite helpful to the understanding of the nuclear charge exchange scattering to take note of the behavior of the free π-N charge exchange cross section. Figure 1 shows the energy dependence of the 0° cross section for the $\pi^- p \rightarrow \pi^0 n$ reaction from 0–1000 MeV. Below 200 MeV this cross section is seen to be sharply energy dependent, and near 50 MeV the cross section nearly vanishes. By way of preview, it is interesting to note that at 50 MeV in DCX reactions the DIAS and GS cross sections reach their maximum values. It will be interesting to compare the shape of the curve in Fig. 1 with that for SCX and DCX in nuclei. SCX is a single scattering process (certainly at low energies) and thus might be expected to follow the π-N curve. DCX is a double scattering process and it may have a different curve. In fact, it is totally different, as we shall see.

Figure 2 shows π-N angular distributions at 50, 180, and 425 MeV. At 50 MeV the cross sections are backward peaked due to the s-p wave interference. At energies above 100 MeV the cross sections have a forward peak. These features play an important role in determining the features of nuclear SCX and DCX cross sections.

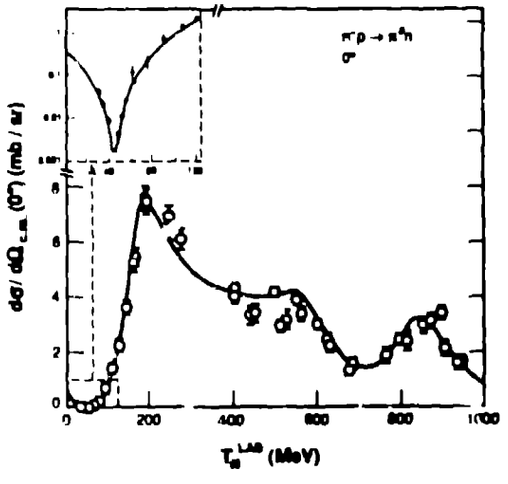

Fig. 1. The differential cross section at 0° for the reaction $\pi^- p \rightarrow \pi^0 n$. The solid line represents a current phase-shift analysis.[1] The inset is taken from Ref. 2.

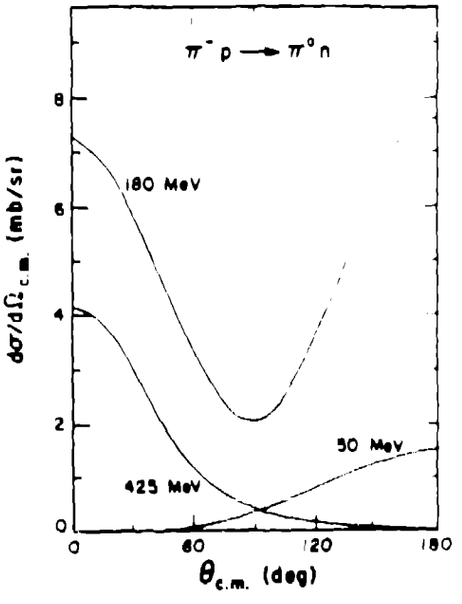

Fig. 2. Angular distribution for the $\pi^- p \rightarrow \pi^0 n$ reaction at three energies, as given by a current phase-shift analysis.[1]

3. π-A SCX Scattering

Figure 3 shows the measured[3] 0° IAS cross section for ^{14}C. The solid curve is the π-N cross section multiplied by 2. We see that this curve tracks closely the measured ^{14}C cross sections up to about 80 MeV. At higher energies the nuclear cross sections fall well below $(N-Z)\cdot\sigma(\pi N)$ cross sections. The theoretical curve by Kaufmann et al.[3] describes well the data up to 300 MeV. We conclude from the ^{14}C data that at low pion energies nuclear SCX is a single scattering process that is not too disturbed by medium effects. At higher energies medium effects suppress the nuclear cross section. These data lend support to the use of the single scattering approximation in theoretical calculations.

Figure 4 shows the measured[4] 0° cross sections for nuclei from ^{7}Li to ^{120}Sn. The curves represent polynomial functions fit to the data to locate the positions of the minima. One can see that the sharp dip structure of the elementary π-N cross section is preserved in the nuclear scattering in nuclei as heavy as $A = 120$.

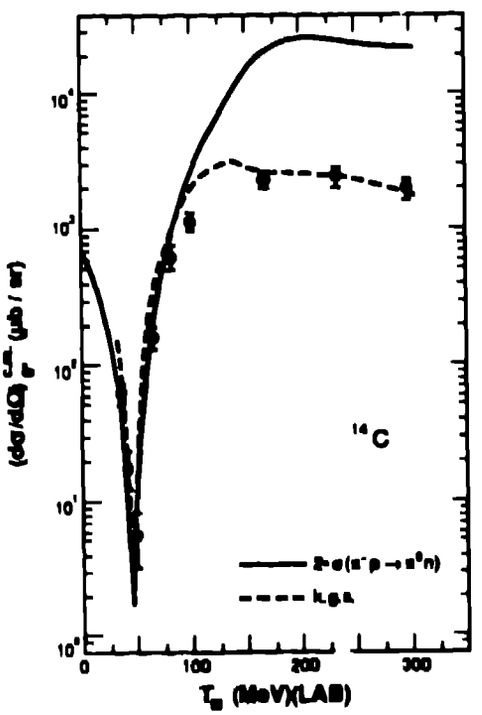

Fig. 3. The energy dependence of the 0° IAS cross section on ^{14}C (Ref. 3). The solid line corresponds to two times the free $\pi^- p \rightarrow \pi^0 n$ cross section. The dashed line represents the multiple scattering theory calculation of Kaufmann et al., as given in Ref. 3.

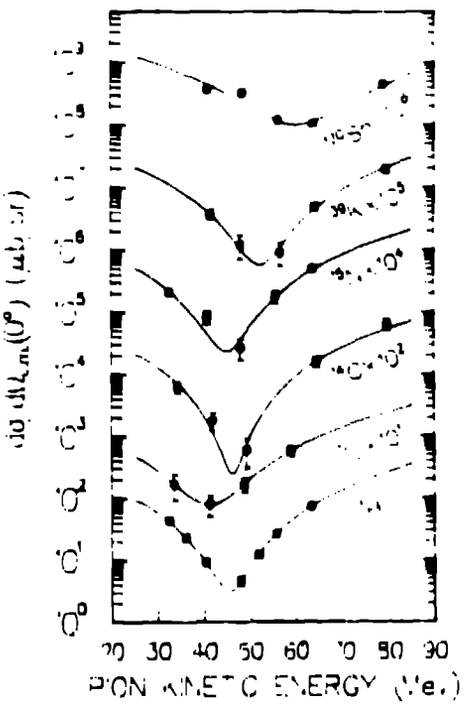

Fig. 4. The measured 0° excitation functions for IAS transitions at low pion energies.[4] The solid lines represent polynomial fits to the data used to determine the energy of the minimum in the cross section.

4. DCX Reaction Mechanisms

Given that forward-angle IAS cross sections appear to be describable in terms of a single scattering on valence nucleons, it is of interest to see if DCX reactions are well described in terms of a double scattering process. If one examines the theoretical literature for the past 20 years, one finds that a simple double scattering picture has not always been assumed. Figure 5 illustrates some DCX mechanisms that have been studied: 6-quark bags,[5,6] delta interactions,[7] and meson-exchange current charge exchange.[8,9] The latter two are discussed at this Workshop by Johnson and Koltun. Also illustrated in Fig. 5 is the sequential double scattering process, which at low energies is a dominant part of the DCX scattering amplitude. There are two sequential scattering amplitudes, one proceeding through the IAS, the other going through nonanalog intermediate states.

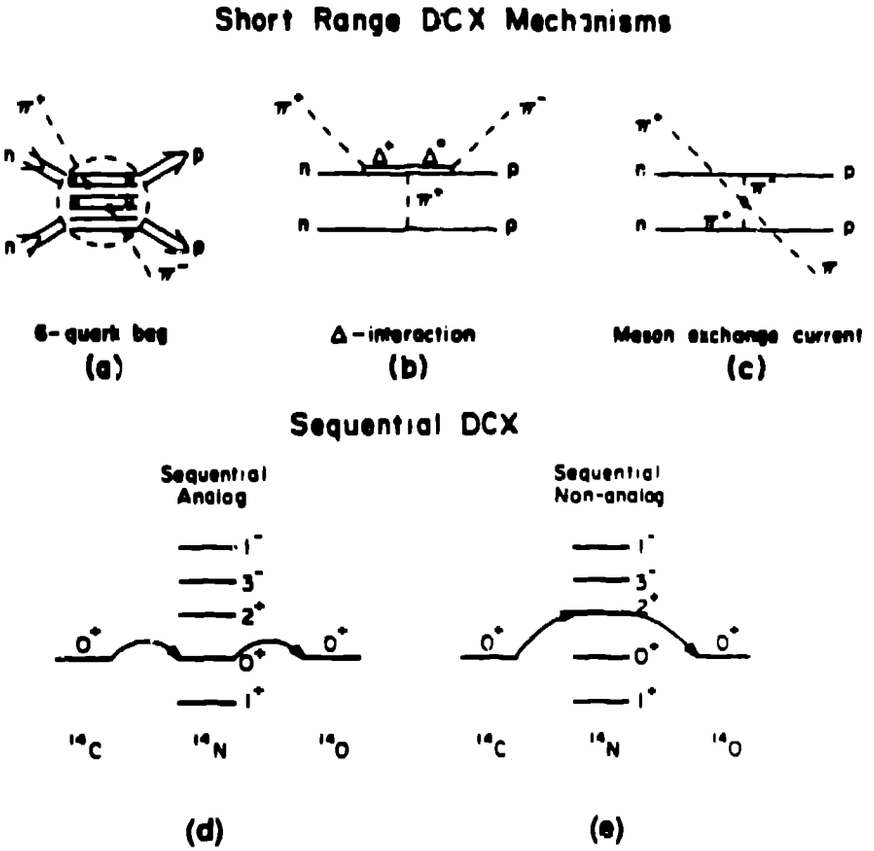

Fig. 5. Illustration of DCX mechanisms that have been employed in the theoretical calculations, and that are discussed in the text.

5. Role of 2-N Correlations in DIAS Transitions on $T = 1$ Nuclei at 50 MeV

The prototype $T = 1$ transition is that of ^{14}C, which has been measured most completely,[10] and which has been the subject of numerous theoretical investigations. Figure 6 shows the SCX and DCX data on ^{14}C and the theoretical calculations of Bleszynski and Glauber.[12] The displayed curves were calculated using single- and sequential-double scattering pictures, respectively, with the Cohen and Kurath wave function[13] for the GS of ^{14}C. Clearly, very good descriptions of both the IAS and DIAS transitions are obtained. Also, a relatively minor role of distortions is indicated.[12]

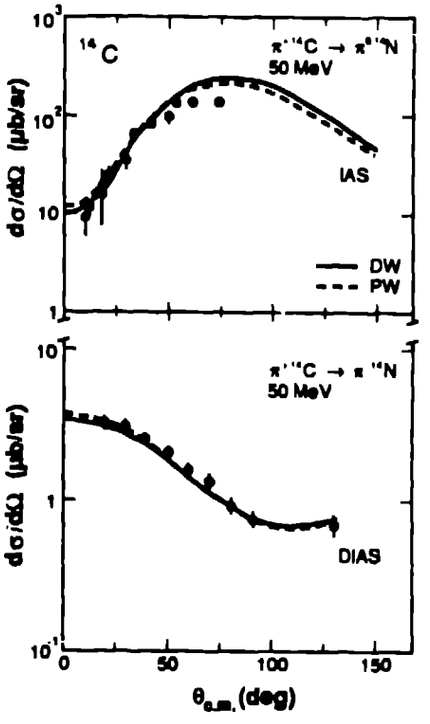

Fig. 6. The data on ^{14}C for the IAS transition[3] and the DIAS transition[11] are compared to the calculations of Ref. 12.

Figure 7 shows how important the geometric correlations in shell-model wave functions are in producing the forward-angle maximum in the DIAS cross sections. The nuclear structure involved in the calculation of DIAS cross section is the pairwise two-body correlation function for an arbitrary pair of valence neutrons. Following Ref. 12, this may be written as

$$\rho^{(2)}(\vec{r}_1, \vec{r}_2) = \rho(r_1)\rho(r_2) + C_{N-Z}(\vec{r}_1, \vec{r}_2) \quad ,$$

where the first term on the right hand side represents independent uncorrelated particle motion, and the second term represents the 2-N correlations. For two nucleons in $\ell = 1$ orbits, it is possible to write the two-particle density function in the form

$$\rho^{(2)}(\vec{r}_1, \vec{r}_2) = N\,\rho(r_1)\rho(r_2)\{a + b\cos^2\theta_{12}\} \quad ,$$

where N is a normalization constant. The values of a and b depend on the assumed GS wave function. The Cohen-Kurath wave function for ^{14}C yields values[14] $(a, b) = (0.393, 1.818)$. The curve in Fig. 7 labeled "correlated nucleons" follows from these values; the curve labeled "independent nucleons" follows from $(a, b) = (1, 0)$.

The extreme sensitivity to values of a and b is illustrated in Fig. 8, taken from Ref. 15. The calculation with $(a, b) = (0, 1)$ gives a very forward-peaked diffraction-like angular distribution shape; whereas the calculation with $(a, b) = (1, 0)$ gives a forward-depressed, featureless, angular distribution. Thus, the geometric features of the two-body density functions play a major role in shaping the DCX cross sections.

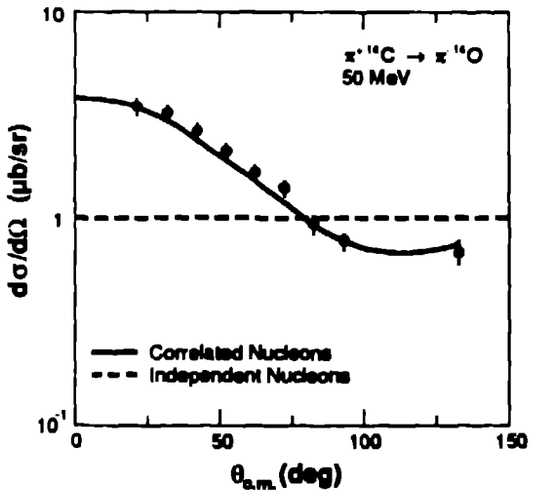

Fig. 7. The calculations of Ref. 12 compared to the DIAS data on ^{14}C from Ref. 11. The two curves demonstrate the importance of including 2-N correlations in the valence nucleons. The correlations result from the Cohen and Kurath wave function[13] for the ^{14}C ground state.

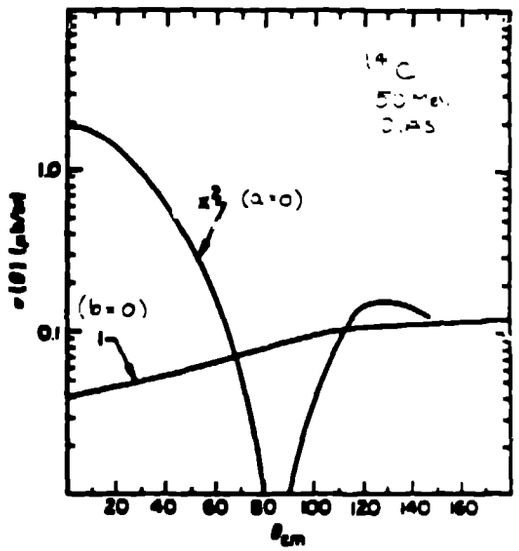

Fig. 8. Calculations of Gibbs et al.[15] illustrating the large effects that 2-N correlations have on DIAS cross sections. The coefficients a and b are defined in the text.

6. A-Dependence of DIAS Cross Sections

There now exist measurements of forward angle DIAS cross sections at 50 MeV on the $T = 1$ nuclei ^{14}C,[11] ^{18}O,[14] ^{26}Mg,[16] ^{34}S,[17] and ^{42}Ca.[18] Figure 9 shows that these DCX cross sections at 50 MeV at 0° are large and nearly independent of A for nuclei from ^{14}C to ^{42}Ca. The near constancy of $T = 1$ cross sections would seem to indicate that the effect of distortions is either small, as suggested in Ref. 12, or weakly A-dependent over this mass region. Furthermore, the 2-N correlations in the valence pair of nucleons would seem to be nearly the same in these $T = 1$ nuclei.

The ^{44}Ca cross section, also shown in Fig. 9, is about half of the $T = 1$ nuclei. This datum was the tell-tale clue on the important role of 2-N correlations, as discussed below. The 50-MeV data are in sharp contrast to the 180-MeV data,

which fall off with the A-dependence of $A^{-10/3}$. This behavior is characteristic of double-forward angle charge-exchange scattering on valence nucleons located on the nuclear surface.[19] The ^{44}Ca cross section at 180 MeV, when divided by the pair factor of 6, falls right on this line. Thus, the data at 180 MeV do not reveal the 2-N correlation effect. We attribute this to the low nuclear penetration at this energy.

7. Results and Analysis of the 35-MeV DIAS Data on the Ca Isotopes

The Ca isotopes have yielded the most direct evidence on the large effect of 2-N correlations on low-energy DCX cross sections. The DIAS and GS transitions involve mainly $1f_{7/2}$ neutrons converted to protons. The comparison of ratios of cross sections across the isotope chain gives an unusually good evaluation of theoretical calculations.

Figure 10 shows the level schemes for ^{42,44,48}Ca as relevant for the IAS, DIAS, and GS transitions. Across the isotope chain the DIAS has approximately the same Q-value of -12.4 MeV. In ^{44}Ti the DIAS is at 9.4 MeV excitation. In ^{48}Ti it is at 17.4 MeV excitation.[20] At low pion energies there exist data on the DIAS and GS transitions but not, unfortunately, on the IAS transitions.

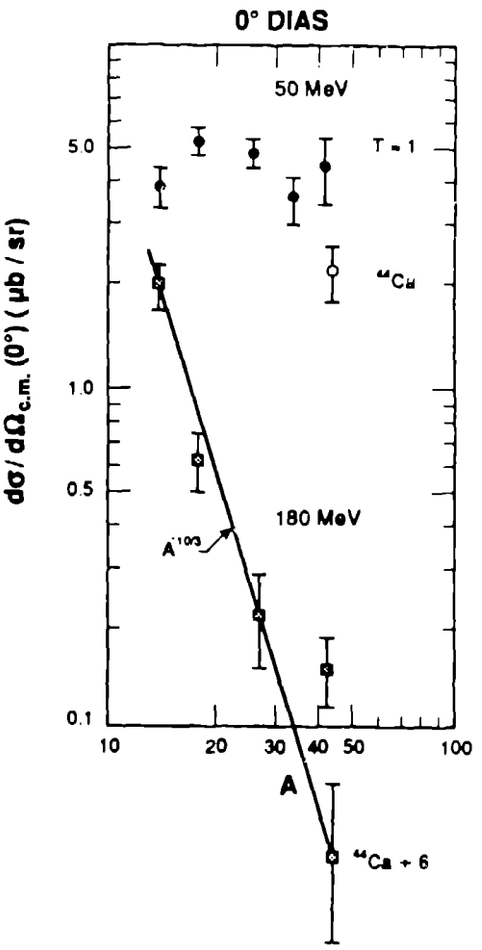

Fig. 9. Forward-angle DIAS cross sections at 50 MeV and at 180 MeV for nuclei ^{14}C, ^{18}O, ^{26}Mg, ^{34}S, ^{42}Ca, and ^{44}Ca. The ^{44}Ca cross section at 180 MeV follows the general pattern of "black disk" scattering. At 50 MeV the ^{44}Ca cross section is quite "anomalous." Its small value is now understood to be due to 2-N correlations, as discussed in the text. Data references are given in the text.

Analyses of the 35-MeV DIAS data[21] were performed by Bleszynski et al.[23] and by Auerbach et al.[24] These have yielded good overall agreement with cross section ratios at forward angles. Also, some success in describing angular distribution shapes is achieved. Figure 11 shows the ^{42,48}Ca data compared with the calculations of Ref. 23. The very different shapes of the two angular distributions

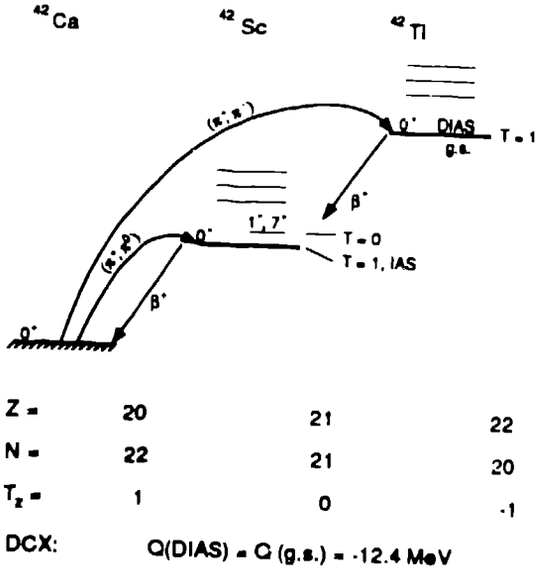

Fig. 10(a). Level scheme for ^{42}Ca as relevant for the IAS and DIAS transitions.

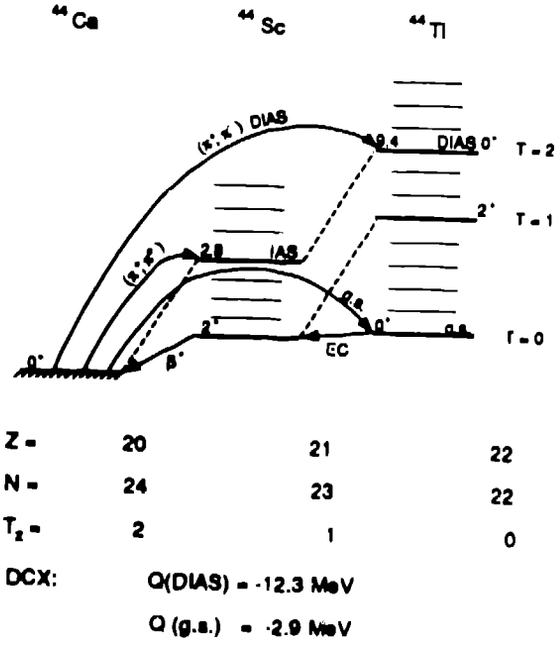

Fig. 10(b). Level scheme for ^{44}Ca as relevant for the IAS, DIAS, and GS transitions.

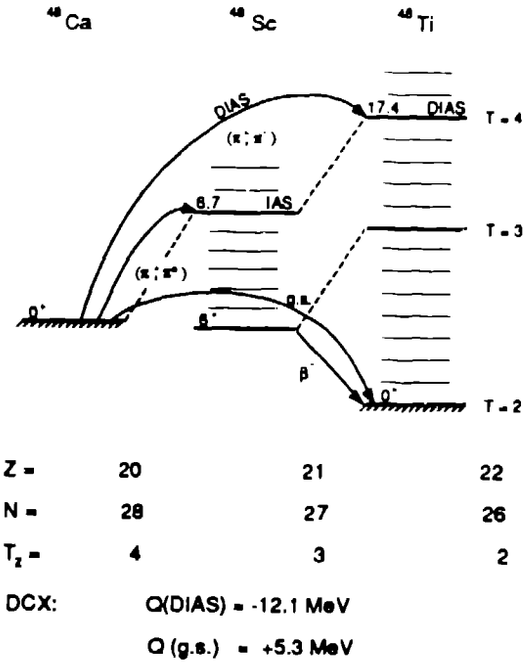

Fig. 10(c). Level scheme for ^{4,5}Ca as relevant for the IAS, DIAS, and GS transitions.

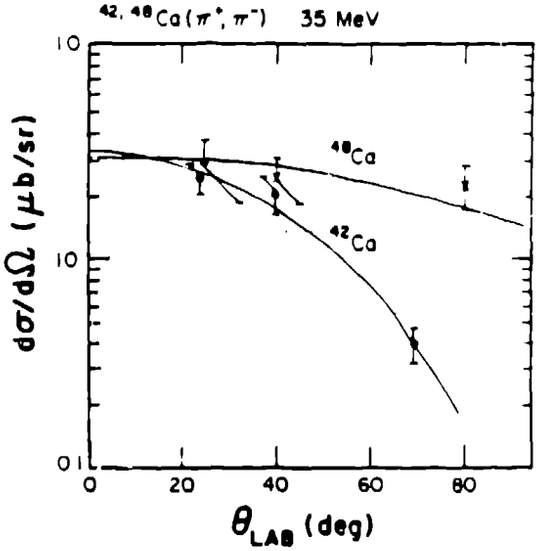

Fig. 11. The measured[21,22] angular distributions for the ^{42,48}Ca(π^+,π^-) DIAS transitions at 35 MeV are compared to the calculations of Ref. 23.

is reproduced. The fact that ^{42}Ca and ^{48}Ca have the same cross section at forward angles, but different angular distribution shapes, follows directly from the 2-N correlations involved.[23] Figure 12 shows the separation densities for a pair of neutrons in ^{42,44,48}Ca, as calculated in Ref. 23. One sees that the probability of finding the two neutrons in ^{42}Ca close together ($r_{12} = 0$) is much larger than in ^{48}Ca or ^{44}Ca. This leads to a much larger cross section per pair for ^{42}Ca than for ^{48}Ca. As shown in Ref. 23, the DCX reaction derives its strength primarily from two closely spaced nucleons.

8. Evaluation of the AGGK Model on $1f_{7/2}$ Shell Nuclei

The "anomalous" cross section ratios on the Ca isotopes led to a more generalized formulation of the DCX transition amplitude first by Auerbach et al.,[25] followed by a generalized version by Auerbach et al.[24] (AGGK). This model is known as the 2-amplitude 0-seniority model for DIAS and GS transitions. In the AGGK formulation, two amplitudes, denoted by A and B, describe all DIAS and GS transitions involving neutrons and protons in a single shell. A detailed evaluation of this model is given in Ref. 21 for the 35-MeV data on ^{42,44,48}Ca, ^{46,50}Ti, and ^{54}Fe. In general, there is good agreement between the model values, with fit values of A, B, and $\cos\theta$, and the experimental values. The fit values of A and B have the ratio $A/B = 3.6 \pm 0.8$ at 25°. This value compares well with the calculated value of Gibbs et al., shown in Fig. 13. Also, Johnson reports a value of A/B at this Workshop, which is close to the empirical value.

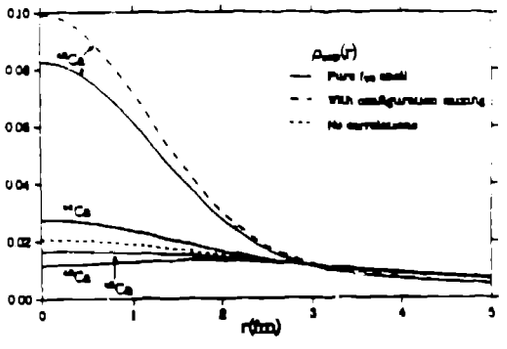

Fig. 12. Separation densities $\rho_{sep}(|\vec{r}_1 - \vec{r}_2|)$ for a pair of valence neutrons in Ca isotopes, as given in Ref. 23.

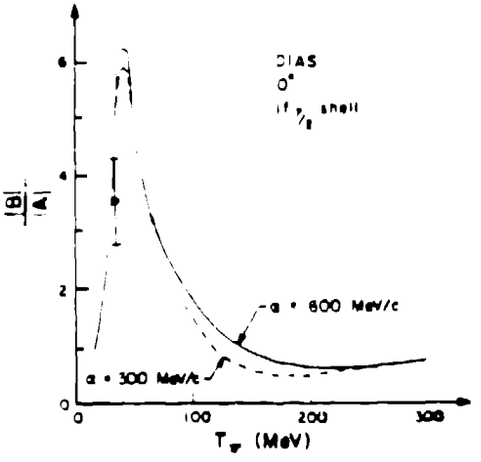

Fig. 13. Theoretical values of the ratio $|A|/|B|$ as a function of pion energy. The scattering amplitudes were calculated according to the model of Ref. 24. The data point at 35 MeV comes from Ref. 21.

9. Energy Dependence of DCX Cross Sections

Figure 14 shows the energy dependence of the forward-angle DIAS cross section between 0 and 500 MeV for ^{14}C, ^{18}O, ^{26}Mg, and ^{42}Ca. One sees that, except for ^{14}C, the largest DIAS cross sections are found around 50 MeV. It is interesting to compare the curves in Fig. 14 with the basic charge exchange curve shown in Fig. 1. The curves are totally different and seem unrelated. The DCX cross sections are very small at resonance energies where the π-N cross sections peak. At higher energies the DIAS cross sections at forward angles are relatively large. In contrast, the cross sections to nonanalog states become very small at the higher energies. At low energies, where the DCX cross section is very small, the DIAS and GS cross sections are at a maximum.

Figure 15 shows the DIAS cross sections for ^{42}Ca and ^{48}Ca and the GS cross section for ^{48}Ca. All these cross sections are seen to have maximum values around

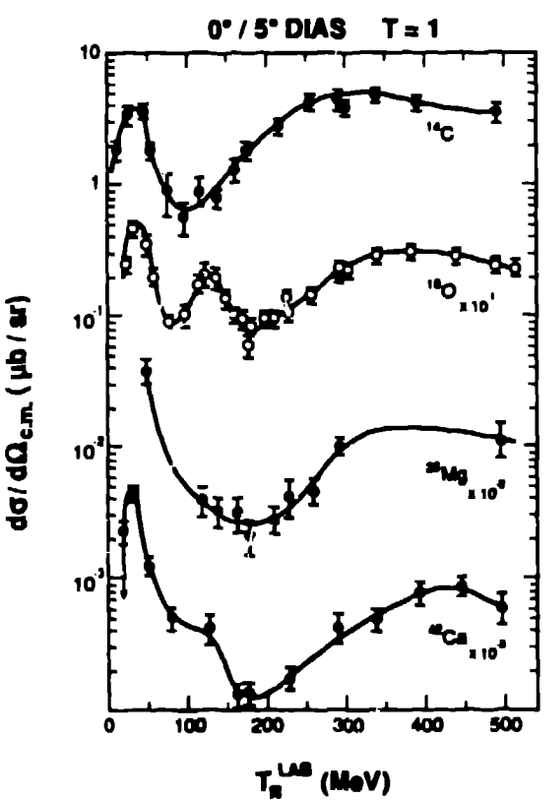

Fig. 14. The measured energy dependence of forward-angle DIAS cross sections for four $T = 1$ nuclei. The solid lines are drawn to guide the eye.

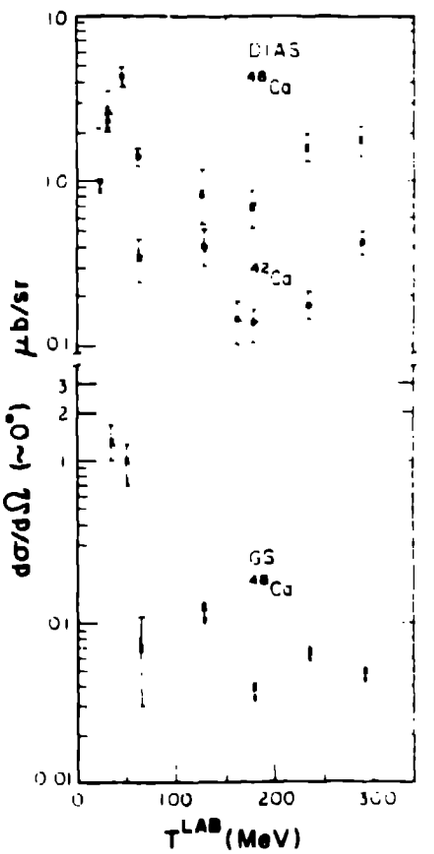

Fig. 15. Energy dependence of DIAS and GS cross sections at 0°/5° for Ca isotopes. Note that the largest cross sections are found at a pion energy near 40 MeV.

40 MeV. At resonance energies all measured GS cross sections drop to a few tenths of a μb/sr or less. At higher energies they drop below 0.3 μb/sr, and have become difficult to measure.

The sharp energy dependence of the DIAS and GS cross sections in the interval 50 to 100 MeV is quite remarkable, and has produced a lot of surprises while taking data. A small change in beam energy can produce a qualitative change in the appearance of the spectra. This is illustrated in Figs. 16(a–f) for ^{44}Ca. Spectra measured at beam energies from 35 to 400 MeV are shown. At energies near 40 MeV both the DIAS and GS are visible [Figs. 16(a) and (b)]. At 65 MeV the DIAS is not visible, although the ground state is quite evident [Fig. 16(c)]; the same is true at 140 MeV [Fig. 16(d)]. At 180 MeV both states are again visible, and both have quite small cross sections. At 260 MeV [Fig. 16(d)], 292 MeV [Fig. 16(e)], and at 400 MeV [Fig. 16(f)] the DIAS stands out clearly in the spectra. At these energies there is no trace of the GS. The features illustrated here for ^{44}Ca hold true generally for the $T \geq 2$ nuclei. This means that the study of GS transitions is best performed at beam energies near 50 MeV.

In the past few years we have made detailed measurements on the energy dependence at low energies of the DIAS and GS transitions on the Ca isotopes. Figure 17 shows these measurements.[30] What we see is a resonance-like shape for both cross sections with a peak near 40 MeV. At or near this energy the theoretical analysis in terms of a sequential scattering with closure on intermediate states has been quite successful.

The observed energy dependence for the Ca isotopes was not anticipated theoretically. Calculations were performed by Gibbs and Kaufmann[31] in parallel with the measurements. Figure 18 shows representative calculations. They show an increase of DIAS cross sections at low energies for ^{44,48}Ca and a nearly flat cross section between 20 and 50 MeV for ^{42}Ca. These predictions are in strong contradiction with the data shown in Fig. 17. These calculations used the AGGK model, which assumes closure on intermediate states, with a fixed energy for the intermediate state. The energy dependence of A and B are shown separately in Fig. 19. From these, one can understand the predicted energy dependence of the cross sections. The relative weightings of the A and B terms in the cross sections are given by $1|A + B|^2$, $6|A + B/9|^2$, and $28|A - B/7|^2$ for ^{42}Ca, ^{44}Ca, and ^{48}Ca, respectively. Thus, the decrease of the B term at the lower energies and the rise of the A term at the lower energies leads to an increase in the predicted ^{44,48}Ca cross sections.

The closure approximation has been questioned recently by Bleszynski and Glauber.[32] In some model calculations for ^{42}Ca, in which they explicitly included intermediate states at different energies, they found the calculated cross sections to fall off at the lowest energies. This result would seem to indicate that a more realistic treatment of intermediate states is needed to describe the observed energy dependence at low energies.

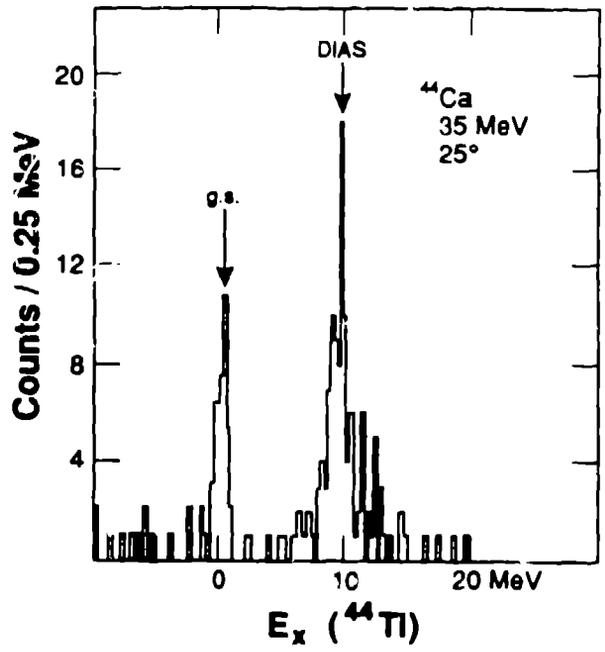

Fig. 16(a). DCX spectrum for ^{44}Ca measured at 35 MeV using the CLAMSHELL spectrometer at LAMPF.[26]

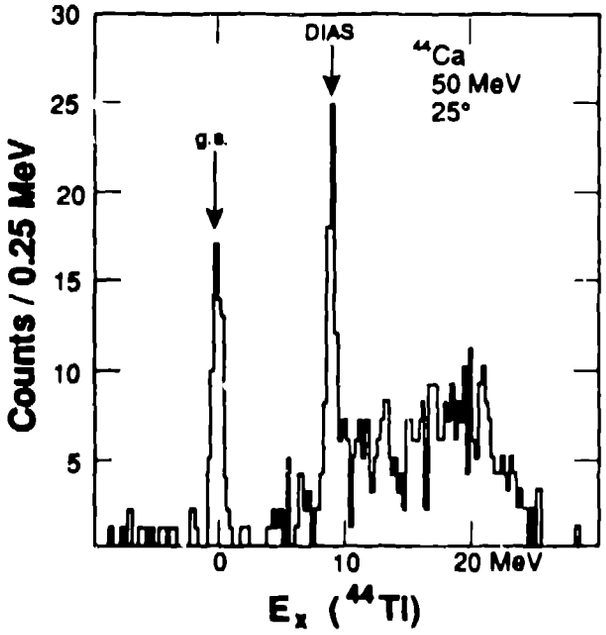

Fig. 16(b). DCX spectrum for ^{44}Ca measured at 50 MeV with the CLAMSHELL spectrometer.[27]

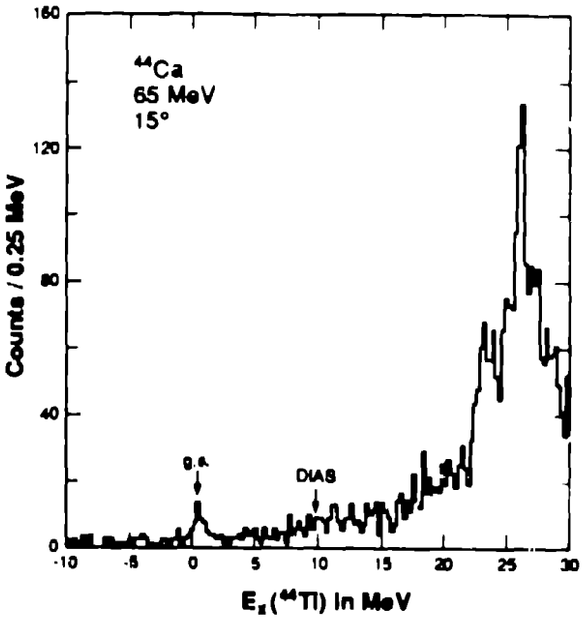

Fig. 16(c). DCX spectrum for ^{44}Ca measured at 65 MeV with the CLAMSHELL spectrometer.[26]

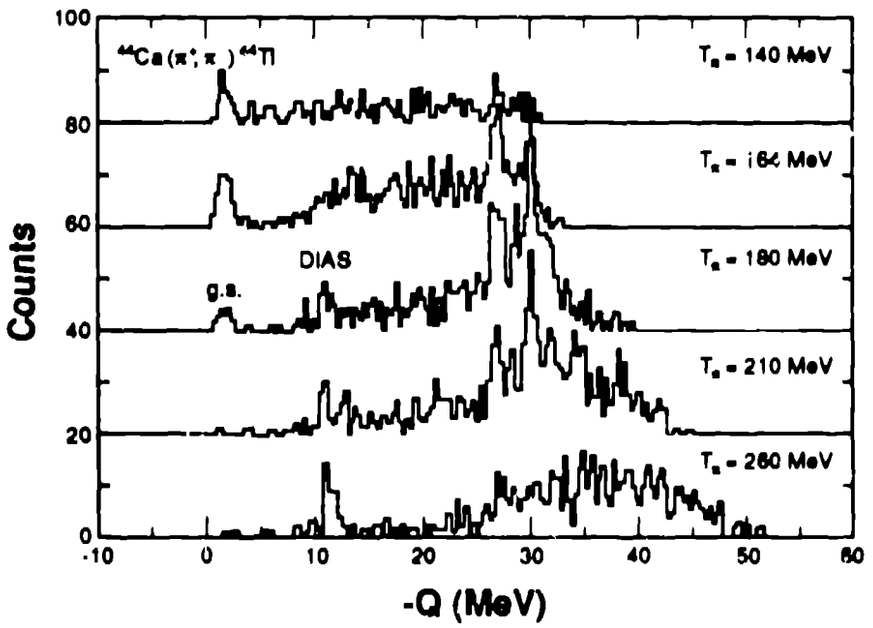

Fig. 16(d). DCX spectra for ^{44}Ca measured[28] at four energies covering the resonance region. Data were measured with EPICS at 5°.

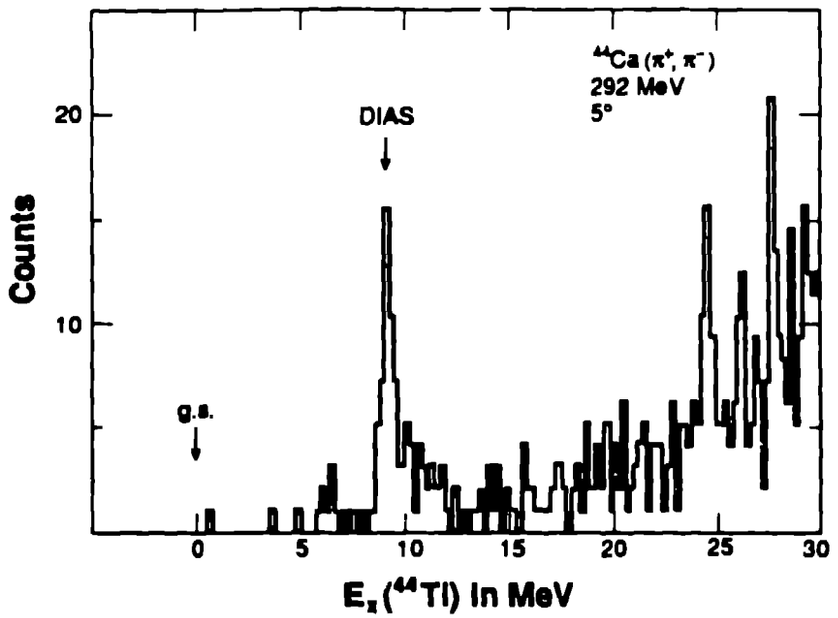

Fig. 16(e). DCX spectrum for ^{44}Ca measured[28] at 292 MeV with EPICS.

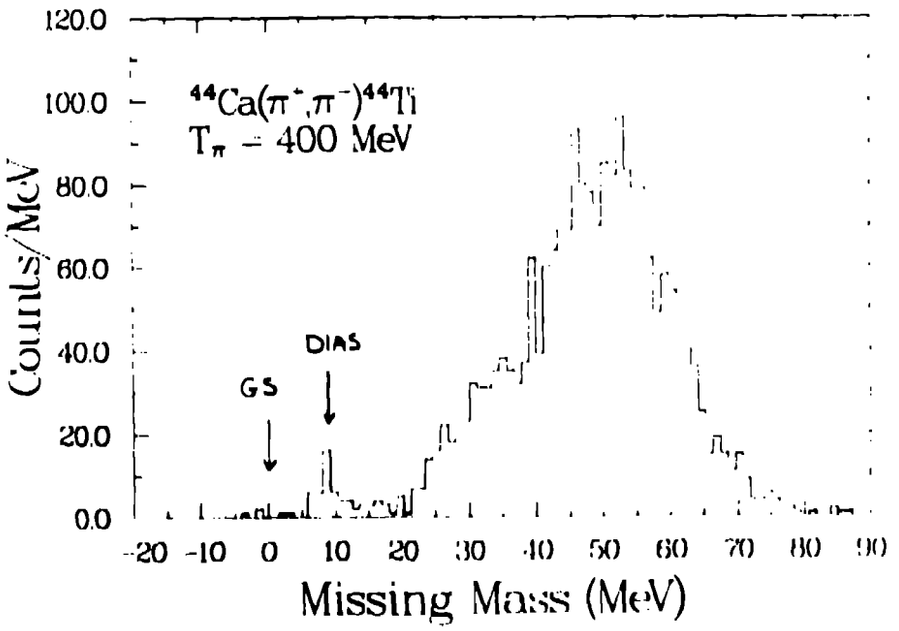

Fig. 16(f). DCX spectrum for ^{44}Ca measured[29] at 400 MeV with the LAS spectrometer at LAMPF.

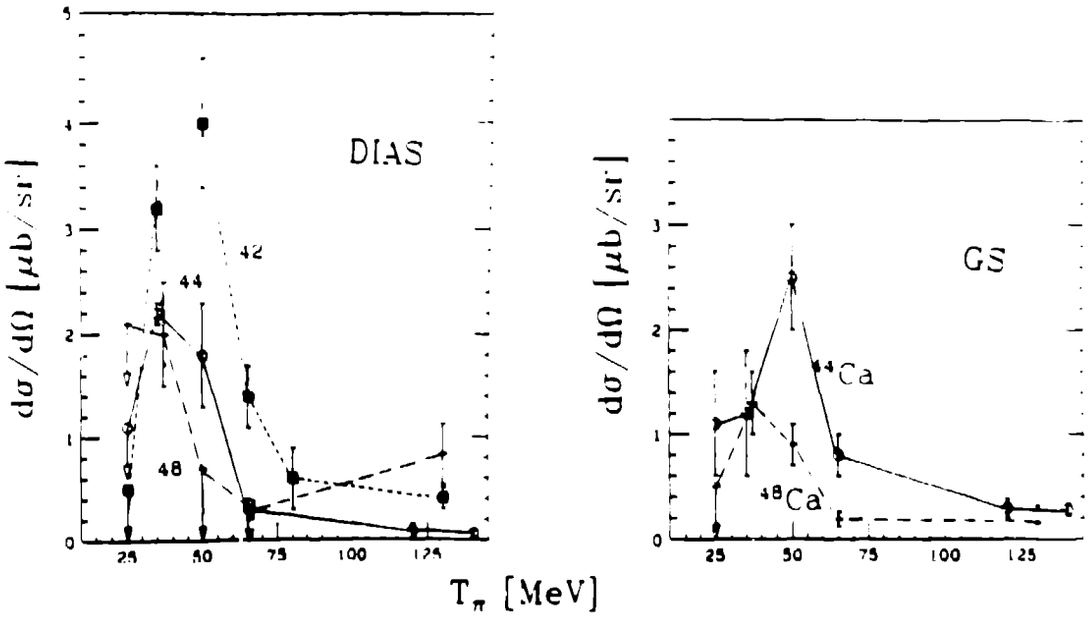

Fig. 17. The measured[30] energy dependence of the forward-angle cross sections for the DIAS and GS in the reactions ^{42,44,48}Ca(π^+,π^-). The lines are drawn to guide the eye.

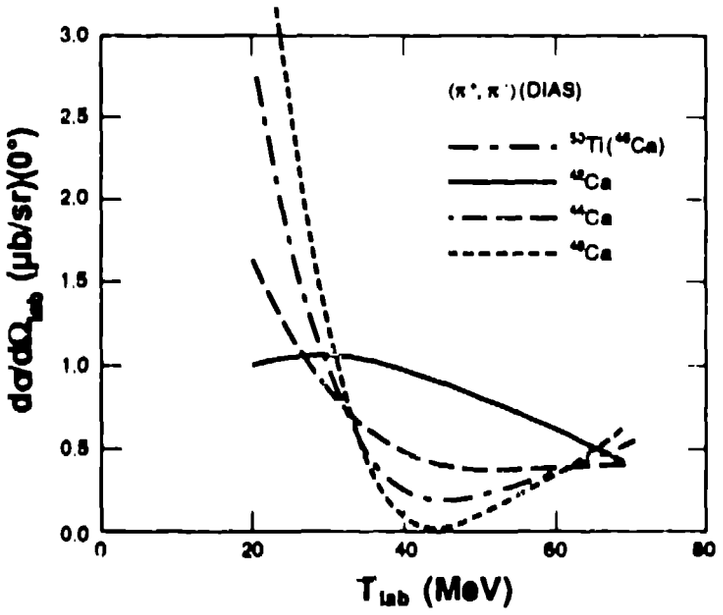

Fig. 18. Calculated[31] energy dependence of the 0° cross sections for the DIAS in the reactions ^{42,44,46,48}Ca(π^+,π^-). The calculations are based on the model of Ref. 24. The rise in cross section at low energies predicted for ^{44,48}Ca is not observed experimentally (see Fig. 17).

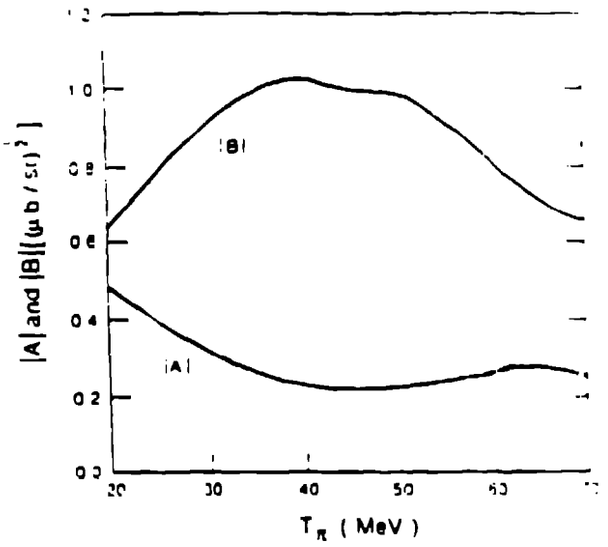

Fig. 19. Calculated[24] energy dependence of the scattering amplitudes $|A|$ and $|B|$ at 0° for $1f_{7/2}$ shell nuclei. The experimental GS cross sections[30] for ^{44,48}Ca follow approximately the shape of $|B|^2$. Also, the measured DIAS cross section[30] for ^{42}Ca follows the $|B|^2$ energy dependence.

Another source of energy dependence in the DIAS cross sections at low energies has been proposed by Siciliano et al.[33] In model calculations for ^{14}C at energies 10 to 110 MeV they show that plane-wave calculations are considerably modified by distortions. In particular, they suggest that distortions will decrease the DIAS cross sections below about 60 MeV. Further studies of this effect are suggested.

10. Summary and Conclusions

At low pion energies:

(1) SCX and DCX are unusually clean manifestations of single and double scattering processes (in hadron-nucleus scattering).

(2) In DCX the large role of 2-N correlations is convincingly demonstrated for a large body of data, for nuclei ranging from ^{14}C to ^{56}Fe.

(3) DIAS and GS cross sections have maximum values near 40 MeV, as found for nuclei with mass up to ^{56}Fe.

(4) DCX is a good probe of nuclear ground state correlations. Two-body nuclear matrix elements of interest to double beta-decay can be studied with DCX.

(5) The energy dependence of DCX cross sections is not well understood.

11. Acknowledgement

I wish to express appreciation to my experimental colleagues on the low-energy DCX program for many enlightening discussions. It has been a pleasure to work with them.Particular thanks go to M. Leitch, E. Piasetzky, and Z. Weinfeld.

12. References

1. Calculated using the π-N phase-shift code SAID, R. Arndt, Virginia Polytechnic Institute and State University.
2. D. H. Fitzgerald et al., *Phys. Rev.* **C34** (1986) 619.
3. J. L. Ullmann et al., *Phys. Rev.* **C33** (1986) 2092.
4. F. Irom et al., *Phys. Rev. Lett.* **55** (1985) 1862.
5. G. A. Miller, *Phys. Rev. Lett.* **53** (1984) 2008.
6. M. B. Johnson and L. S. Kisslinger, *Phys. Lett.* **168B** (1986) 26.
7. A. Wirzba et al., *Phys. Rev.* **C40** (1989) 2745, and references cited.
8. E. Oset et al., *Nucl. Phys.* **A408** (1983) 461.
9. M. F. Jiang and D. S. Koltun, *Phys. Rev.* **C42** (1990) 2662, and references cited.
10. M. J. Leitch et al., *Phys. Rev.* **C39** (1989) 2356.
11. M. J. Leitch, *Phys. Rev. Lett.* **54** (1985) 1482.
12. M. Bleszynski and R. Glauber, *Phys. Rev.* **C36** (1987) 681.
13. S. Cohen and D. Kurath, *Nucl. Phys.* **73** (1965) 1.
14. A. Altman et al., *Phys. Rev. Lett.* **55** (1985) 1273.
15. W. R. Gibbs et al., in *Proceedings of the LAMPF Workshop on Pion Double Charge Exchange*, January 1985, Los Alamos National Laboratory report LA-10550-C (H. W. Baer and M. J. Leitch, eds.), p. 90.
16. T. Anderl, Ph.D. Dissertation, 1987, Universität Bonn (unpublished).
17. R. Bilger et al., Univ. of Tübingen preprint (1991).
18. K. K. Seth, *Nucl. Phys.* **A478** (1988) 591c.
19. M. B. Johnson, in *LAMPF Workshop on Pion Single Charge Exchange*, January 1979, Los Alamos Scientific Laboratory report LA-7892-C (H. W. Baer, J. D. Bowman, and M. B. Johnson, eds.), p. 343.
20. R. T. Kouzes et al., *Nucl. Phys.* **A309** (1978) 329.
21. Z. Weinfeld et al., *Phys. Lett.* **B237** (1990) 33.
22. H. W. Baer et al., *Phys. Rev.* **C35** (1987) 1425.
23. E. Bleszynski et al., *Phys. Rev. Lett.* **60** (1988) 1483.
24. N. Auerbach et al., *Phys. Rev.* **C38** (1988) 1277.
25. N. Auerbach et al., *Phys. Rev. Lett.* **59** (1987) 1076.
26. Z. Weinfeld et al., to be published.
27. H. W. Baer et al., *Phys. Rev.* **C43** (1991) 1458.

28. P. A. Seidl et al., *Phys. Rev.* **C42** (1990) 1929: Fig. 16(d) provided courtesy of C. L. Morris; Fig. 16(e) provided courtesy of R. Gilman.
29. A. L. Williams, *Phys. Rev.* **C43** (1991) 766; Fig. 16(f) provided courtesy of A. L. Williams.
30. Z. Weinfeld et al., contributed abstract to this Workshop; and, to be published.
31. Calculations were performed by Gibbs and Kaufmann based on model of Ref. 23. They are shown in LAMPF Proposal #1098.
32. M. Bleszynski and R. Glauber, presented at the Second Workshop on Pion-Nucleus Double Charge Exchange, April 1989, Los Alamos, New Mexico.
33. E. R. Siciliano et al., *Ann. Phys.* **203** (1990) 1.